Radiative Rotational Lifetimes and State-Resolved Relative Detachment Cross Sections from Photodetachment Thermometry of Molecular Anions in a Cryogenic Storage Ring

C. Meyer,[1,†] A. Becker,[1] K. Blaum,[1] C. Breitenfeldt,[1,2] S. George,[1] J. Göck,[1] M. Grieser,[1] F. Grussie,[1] E. A. Guerin,[1] R. von Hahn,[1] P. Herwig,[1] C. Krantz,[1] H. Kreckel,[1] J. Lion,[1] S. Lohmann,[1] P. M. Mishra,[1] O. Novotný,[1] A. P. O'Connor,[1] R. Repnow,[1] S. Saurabh,[1] D. Schwalm,[1,3,*] L. Schweikhard,[2] K. Spruck,[1,4] S. Sunil Kumar,[1] S. Vogel,[1] and A. Wolf[1]

[1]*Max-Planck-Institut für Kernphysik, D-69117 Heidelberg, Germany*
[2]*Institut für Physik, Ernst-Moritz-Arndt-Universität Greifswald, D-17487 Greifswald, Germany*
[3]*Weizmann Institute of Science, Rehovot 76100, Israel*
[4]*Institut für Atom- und Molekülphysik, Justus-Liebig-Universität Gießen, D-35392 Gießen, Germany*

(Received 20 April 2017; published 14 July 2017)

Photodetachment thermometry on a beam of OH^- in a cryogenic storage ring cooled to below 10 K is carried out using two-dimensional frequency- and time-dependent photodetachment spectroscopy over 20 min of ion storage. In equilibrium with the low-level blackbody field, we find an effective radiative temperature near 15 K with about 90% of all ions in the rotational ground state. We measure the $J = 1$ natural lifetime (about 193 s) and determine the OH^- rotational transition dipole moment with 1.5% uncertainty. We also measure rotationally dependent relative near-threshold photodetachment cross sections for photodetachment thermometry.

DOI: 10.1103/PhysRevLett.119.023202

Small molecular ions and their interactions in the lowest rotational states are crucial for the formation of molecules in interstellar space and for low-temperature plasma chemistry in general [1,2]. Both cations and anions [3] were observed in space based on rotational spectroscopy. While line positions have been well studied in the laboratory for many relevant ions, experimental information on their line intensities is scarce. Instead, line strengths for ionic rotational transitions are generally obtained from calculated molecular dipole moments. This is mainly due to difficulties of performing absolute laboratory measurements on the dipole moment in the presence of an ionic charge, small radiative absorption in dilute ionic targets, and long natural lifetimes of rotational levels. Recently, cryogenic storage rings for fast ion beams were taken in operation [4,5] that allow the low-lying rotational levels in small molecular ions to relax by spontaneous emission toward equilibrium with a low-temperature blackbody radiation field [6]. In this Letter, we show that near-threshold photodetachment can be used to follow the *in vacuo* rotational relaxation over times long compared to the natural lifetime of the first excited rotational level, and obtain Einstein coefficients for the lowest rotational transitions of the OH^- molecular anion. The measured electric dipole moment differs significantly from the theoretical values available.

Photodetachment experiments on molecular anions reveal a wealth of information on their structure and reactive dynamics. At photon energies close to the electron binding energy, the detachment cross section is a powerful probe for the internal states of the anion and the neutral daughter molecule as well as for the interaction of the outgoing low-energy electron with the neutral molecule. With its simple rotational structure in the $^1\Sigma^+$ ground state, OH^- has been intensely studied, a particular focus being the strong deviations from the Wigner threshold law in the photon energy dependence [7,8]. Although until now significant uncertainties have remained in predicting the cross sections, rotational level distributions in the anion have been characterized using the threshold structure [9,10]. In a cold ion-trap environment, near-threshold photodetachment was applied as a method for rotational thermometry on OH^- anions under buffer-gas cooling [11,12]. In these studies, the relative photodetachment cross sections for the various initial- and final-state-dependent thresholds were the main uncertainty in deconvoluting the rotational population fractions of OH^- from the measured photodetachment rates. In the present Letter we find that probing the radiative rotational relaxation of OH^- offers a way to obtain the convolution parameters of near-threshold photodetachment thermometry consistently on an experimental basis. Hence, in addition to the rotational lifetime measurements, we also determine relative photodetachment cross sections over a sample of near-threshold energies for individual rotational levels of OH^-.

In the present experiment, a beam of OH^- anions from a Cs sputter ion source (expected rotational temperature of a few thousand K [13]) is accelerated to 60 keV and injected into the cryogenic storage ring (CSR) [5]. About 10^7 ions are stored at an ambient temperature near 6 K and a residual gas density corresponding to $< 10^{-14}$ mbar room-temperature pressure. The ion storage time up to 1200 s covers the spontaneous decay of low-lying excited J levels of OH^-

(∼21 and ∼190 s for $J = 2$ and 1, respectively, while vibrations radiatively decay within < 1 s [14]). In a field-free straight section, laser beams are overlapped with the ion beam in a copropagating direction at a grazing angle of 3.4°. With laser and ion beam diameters of ∼7 and ∼30 mm, respectively, the interaction zone is ∼50 cm long. The fast particles neutralized by photodetachment leave the closed orbit of the CSR and are counted by a large microchannel plate detector ∼3 m downstream from the interaction region. A continuous-wave helium-neon (HeNe) laser at 633 nm with an effective power of 0.7 mW in the interaction region yields a steady small rate of photodetachment events. Doppler shifted to the OH^- rest-frame, its wave number is $\tilde{\nu}_r = 15754\ \mathrm{cm}^{-1}$, which is ∼1000 cm^{-1} above the first OH^- ($J = 0$) detachment threshold ($\tilde{\nu}_{EA} = 14741.0\ \mathrm{cm}^{-1}$) corresponding to the ground-state electron affinity [9,10]. Measurements with buffer-gas cooled OH^- ions [15] near 15 106 cm^{-1} and 15 803 cm^{-1} showed that the photodetachment cross section is independent (within ∼10%) of the rotational temperature between 8 and 300 K. Given these small variations of the photodetachment cross section with J, we use the photodetachment rate at $\tilde{\nu}_r$ as a reference signal for the number of OH^- ions in the laser interaction zone. The decay of this signal as a function of time is close to exponential with a time constant of 607(2) s at > 150 s (only $J = 0$ and 1 surviving). By searching for a component in this signal due to the $J = 1$ decay, we find that the relative difference between the photodetachment cross sections of these two states is $< 3\%$.

With the signal at $\tilde{\nu}_r$ for normalization, we measure the neutral rates from a second, probing laser. At similar interaction geometry as the HeNe reference laser, pulses with ∼0.5 mJ, 3–5-ns duration, and a repetition rate of 20 s^{-1} are applied by a tunable pulsed optical parametric oscillator (OPO) laser (EKSPLA NT342B). Close to the excited-J photodetachment thresholds, up to 10 probing wave numbers $\tilde{\nu}_k$ ($k = 1, \ldots, 10$, given in the OH^- rest-frame) are used. The neutrals reach the detector within ∼5 μs after the laser pulses, reflecting the particle flight times. Their counts in a suitable delay window are accumulated as the signal $N(\tilde{\nu}_k, t)$, where t is the time after the ion beam injection. Similarly, the counts due to the HeNe laser are accumulated during the breaks between the laser pulses and recorded as the reference $N(\tilde{\nu}_r, t)$. Laser pulsing starts a few ms after injection. Probing wave numbers $\tilde{\nu}_k$ are cycled through, with typically 100 laser pulses at a single value. The ion beam was dumped 31, 300, or 1200 s after injection. For a run, many of such injections and observation periods were repeated. The starting value of the $\tilde{\nu}_k$ cycle was varied to realize a two-dimensional spectroscopy scheme that applies all probing wave numbers to all beam storage times with a suitable time binning.

For the design of the experiment and the basic understanding of its results, modeling of OH^- near-threshold photodetachment [9,16] was crucial. Starting from $OH^-(J)$, s-wave photodetachment can leave the OH radical ($X^2\Pi$) in up to eight final levels, each forming a threshold j at wave number $\tilde{\nu}_j$. (For $J = 0$, only three thresholds are allowed.) The near-threshold detachment rate is described [17] by a Wigner-type dependence $I_j(\tilde{\nu} - \tilde{\nu}_j)^a$ where, in laser measurements just above threshold, appropriate values of a were found to vary from one threshold to the next with a typical range of $a \approx 0.20, \ldots, 0.25$. The threshold intensities I_j follow from the angular momenta and the OH fine-structure mixing [10,17], in reasonable agreement with the observations. Much less is known about the validity of the threshold power law at higher above-threshold photon energies ($\tilde{\nu} - \tilde{\nu}_j$), which in photodetachment thermometry can reach up a few hundred cm^{-1}. Our data analysis is largely independent of a photodetachment cross section model and we obtain the J-dependent relative cross sections from the time dependence at the various probing wave numbers $\tilde{\nu}_k$. We have to relate only one of the J-dependent cross sections at a single $\tilde{\nu}_k$ to the reference rate via the cross-section model. Moreover, unresolved contributions of higher J (≥ 4) are included based on the model results. Specifically, the analytical model for a threshold j is chosen as $\sigma_j(\tilde{\nu}) = \hat{I}_j(\tilde{\nu} - \tilde{\nu}_j)^a(\tilde{\nu}/\tilde{\nu}_j)^{b-a}$ with $\hat{I}_j = I_j/(2J + 1)$ [18]. A factor of power $b - a$ is introduced to model cross-section deviations from the threshold law at higher $\tilde{\nu}$. Few data [15,27] are available for the cross section in this $\tilde{\nu}$ range and indicate a maximum at, roughly, 16 000 cm^{-1}. We choose $a = 0.20$ and $b = -2.8$ for a model approximating the photon energy dependence.

The cross-section model for $OH^-(J)$ is obtained as $\sigma_J(\tilde{\nu}) = \sum_{j(J)}\sigma_j(\tilde{\nu})$, where $j(J)$ denotes all thresholds for a given J. For OH^- with a rotational temperature T the cross section (Fig. 1) is the average over $\sigma_J(\tilde{\nu})$ with the

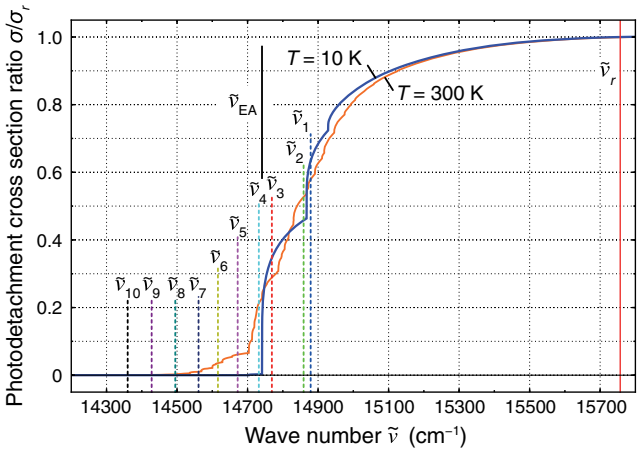

FIG. 1. Near-threshold photodetachment cross section of OH^- modeled by $\sigma_T(\tilde{\nu}; T) = \sum_J p_J(T)\sigma_J(\tilde{\nu})$ with $\sigma_J(\tilde{\nu})$ for $a = 0.20$, $b = -2.8$, and for $T = 10$ K and 300 K as labeled. The reference cross section is $\sigma_r = \sigma_{J=0}(\tilde{\nu}_r)$ at the HeNe laser wave number (full vertical mark, see the text). Probing wave numbers $\tilde{\nu}_k$ are indicated by dashed marks.

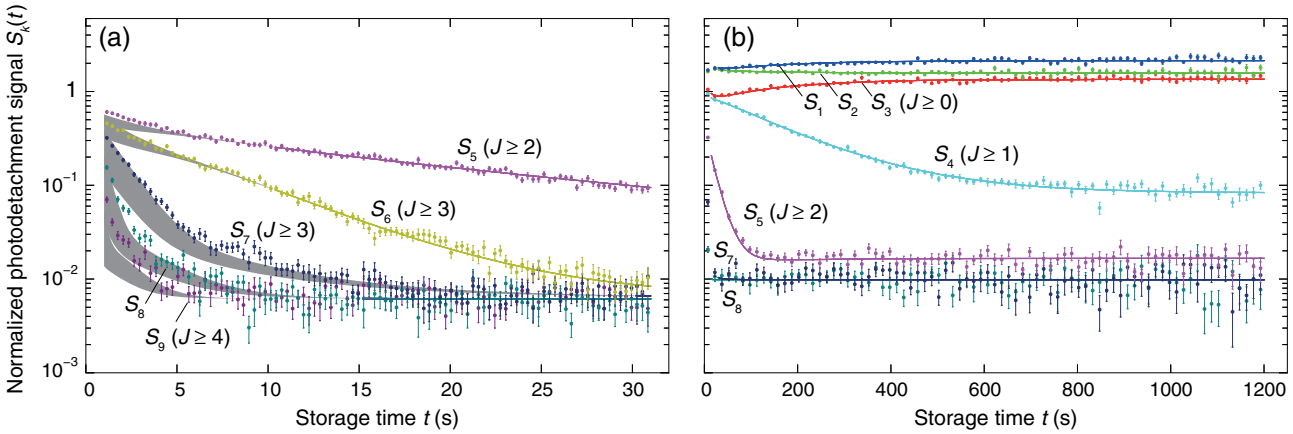

FIG. 2. Photodetachment signals $S_k(t) = N(\tilde{\nu}_k, t)/N(\tilde{\nu}_r, t)$ as functions of the ion storage time for two sample runs with 1151 (a) and 38 (b) injections. Ranges of J levels contributing to the signals are marked. Data points represent the measured count ratios and their 1σ uncertainties. The full lines show a fit to the signals of all runs using the modeled photodetachment cross sections and level populations. In (a) the shaded areas indicate the model variation with T_0 at the short times when the data were excluded from the fit (see text).

population probabilities p_J. For $T = 10$ K, it is dominated by $J = 0$ ($p_0 = 0.987$) with a rise at $\tilde{\nu}_{\mathrm{EA}}$ followed by two further thresholds within the next 200 cm^{-1}. Higher J levels populated at $T = 300$ K lead to a broadening of the threshold structures, while from ~600 cm^{-1} above $\tilde{\nu}_{\mathrm{EA}}$ the cross sections are largely independent of T and J.

Among the probe wave numbers, $\tilde{\nu}_1, \ldots, \tilde{\nu}_3$ lie well above $\tilde{\nu}_{\mathrm{EA}}$ (Fig. 1) and, thus, yield contributions from all $J \geq 0$. Other $\tilde{\nu}_k$ successively exclude low-J levels; contributing J s are, e.g., $J \geq 1$ for $\tilde{\nu}_4$ and $J \geq 2$ for $\tilde{\nu}_5$. Signals $S_k(t) = N(\tilde{\nu}_k, t)/N(\tilde{\nu}_r, t)$, shown in Fig. 2, are obtained by normalizing the counts $N(\tilde{\nu}_k, t)$ to the reference $N(\tilde{\nu}_r, t)$. A short run up to 31 s, using $\tilde{\nu}_5, \ldots, \tilde{\nu}_9$, shows the successive cooling of higher rotational levels. After the fast decay of $J \geq 4$ ($t \gtrsim 10$ s), S_6 essentially shows the relaxation of $J = 3$. Similarly, S_5 at later times ($\gtrsim$30 s) represents the $J = 2$ decay. In a long run up to 1200 s, S_4 for $t \gtrsim 200$ s represents the pure $J = 1$ decay. Furthermore, the signals $S_1, \ldots, S_3$ clearly show the different J contributions by their characteristic time dependences consistent with S_4 and S_5, in particular.

The normalized signals represent a convolution of the time-dependent J-level populations p_J with a matrix representing the relative photodetachment cross sections at the probing wave numbers, $S_k(t) = S_0 \sum_J p_J(t) \phi_k \sigma_J(\tilde{\nu}_k)/\sigma_r$. Factors ϕ_k close to 1 describe the small relative variations of the OPO laser flux over $\tilde{\nu}_k$ (known within ~3%). The OH^- radiative relaxation can be well described by only a few parameters: the Einstein coefficients A_J for transitions $J \to J-1$, the photon occupation numbers $n(\tilde{\nu}_J)$ of the ambient radiation field at the transition energies $\tilde{\nu}_J$ for transitions $J \to J+1$, and the initial populations p_J^0 of the rate model [18]. An overall scaling parameter S_0 (in the range of 3.4 to 4.4) takes into account the integrated powers and the slightly different overlaps of the two laser beams.

The signals $S_k(t)$ were fitted by a single model simultaneously for all runs. We assume that the $n(\tilde{\nu}_J)$ are given by a radiative temperature T_r according to Bose-Einstein statistics. The populations p_J^0 from the excitation in the ion source are described by a temperature T_0. We independently varied in the fit all A_J for $J \leq 3$. At the various $\tilde{\nu}_k$, the signal variations differently reflect the radiative time constants and the J-dependent photodetachment cross sections $\sigma_J(\tilde{\nu}_k)/\sigma_r$. Hence, the relative cross sections can also be obtained.

We fit $S_{1,2}$ for $t > 30$ s and S_3 to S_6 for $t > 10$ s to determine relative σ_J values for $J = 0$ to 3. The time limits are set to safely ensure the decay of higher-J levels. On the other hand, the radiative lifetimes of $J = 1$ to 3 are sensitively probed. For fitting S_0, one of the relative photodetachment cross sections, for which we chose $\sigma_{J=0}(\tilde{\nu}_3)/\sigma_r$, has to be set to its calculated value. In S_7 to S_{10}, contributions from various higher J s overlap at shorter times. We do not fit these short-time data, but only compare them to the model using the calculated $\sigma_J(\tilde{\nu}_k)/\sigma_r$. The higher-$J$ lifetimes are set according to the relation $A_J = 16\pi^3 \tilde{\nu}_{J-1}^3 \mu_0^2 J/3\epsilon_0 h(2J+1)$ [23] using the dipole moment $\mu_{0,J\geq 3}$ from the fitted $J = 3$ lifetime. The backgrounds in these data are fitted for $t > 15$ s ($t > 30$ s for S_7). Separate fits were performed setting the start temperature T_0 between 1000 and 6000 K. Within the fitted time ranges the model curves and the fitted parameters remain essentially unchanged. In the short-time ranges excluded from the fits the results vary significantly. This is indicated by shaded areas in Fig. 2(a). Their upper edges, representing the model for $T_0 = 6000$ K, yield best agreement with the data. Hence, we give the results for the fit at $T_0 = 6000$ K and consider the estimated parameter variations over a range of ± 2000 K in T_0 as a systematic uncertainty. The reduced mean-squared residuals χ_r^2 were close to 1.30 in all cases.

Two further experimental features were included in the fit. First, a small fraction of $^{17}O^-$ ions of $(1.7, \ldots, 5.9) \times 10^{-3}$ [18] occurred in the stored OH^- beam and, for the O^- electron affinity near 11 784.7 cm^{-1} [28], led to a small constant neutralization background even for the probing lines far below the OH^- threshold. It was considered as a constant background in $S_k(t)$ with independent values for different runs. Moreover, reflection of laser light at the downstream vacuum window produced a small additional probing-light component Doppler shifted by $\tilde{\nu}'_k - \tilde{\nu}_k \approx +80$ cm^{-1}. This yields a small contribution from $J = 0$ ions in S_5 (probing $J \geq 2$) slightly shifting the S_5 equilibrium level in Fig. 2(b). The weak, Doppler-shifted reflected lines ($\tilde{\nu}'_k$) are consistently included in the model [with theoretical $\sigma_J(\tilde{\nu}'_k)/\sigma_r$] and the reflection factors (up to a few percent) are allowed to vary between different runs. In the fit results, systematic uncertainties due to the starting temperature T_0 have a few-percent effect on the relative cross sections, while they are negligible for the radiative decay and the equilibrium population. The estimated limits for rotational variations of the reference photodetachment cross section and differences in depleting the various J levels by laser photodetachment introduce [18] systematic uncertainties on the radiative decay rates which are included in the overall uncertainty limits of the results.

The fits shown in Fig. 2 yield precise details on the radiative equilibrium in the low-level blackbody field of the CSR, the relative probing cross sections, and the radiative decay rates of the OH^- ion. From the fitted photon occupation number at the $J = 0 \rightarrow 1$ transition frequency in OH^- (37.47 cm^{-1}), we obtain an effective radiative temperature of $T_r = 15.1(1)$ K. Considering the CSR vacuum-chamber temperature [5] near 6 K, the effective relative contribution from room-temperature surfaces to the radiation field is found [18] to be $5.7(2) \times 10^{-3}$.

The fit results for the state-selected relative photodetachment cross sections at the various probe wave numbers are shown in Fig. 3. It is clearly visible that the simple model is inappropriate for the probing energies of 100 cm^{-1} or more above the lowest thresholds in $J = 0$ to 2. As a simple change of the common exponent a of all threshold laws does not improve the overall agreement, the results call for more detailed cross-section calculations beyond simple power-law models. But the experimental cross-section ratios (see listing in Ref. [18]) can directly serve for future photodetachment thermometry, deducing rotational populations from relative photodetachment rates on a theory-independent basis. This will include ion trap experiments such as those of Refs. [11,12], where photodetachment thermometry serves to study cold inelastic collisions by laser depletion of rotational levels.

Results for the Einstein coefficients and the molecular dipole moments are listed in Table I. To our best knowledge, direct *in vacuo* lifetime measurements on low-lying, purely rotationally excited states in small molecules have not been

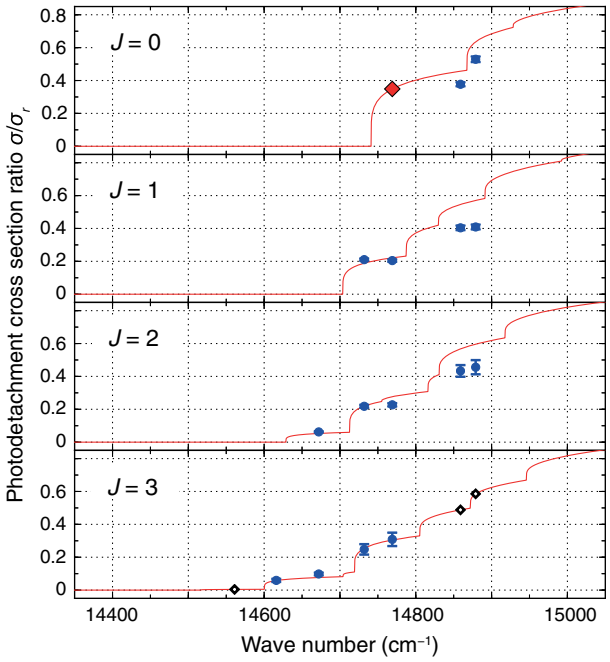

FIG. 3. Near-threshold photodetachment cross section ratios $\sigma_J(\tilde{\nu})/\sigma_r$ of OH^- for the probing lines ($\tilde{\nu} = \tilde{\nu}_k$) determined from the fit (filled symbols with overall 1σ, statistical, and systematic uncertainties) and the model with $a = 0.20$, $b = -2.8$ (full lines). Open diamonds mark theoretical values of $\sigma_J(\tilde{\nu}_k)/\sigma_r$ for the channels where separate features cannot be identified in the data. The model value of $\sigma_{J=0}(\tilde{\nu}_3)/\sigma_r$ serving as a reference (see text) is marked by the large diamond.

reported previously. As expected at the given accuracy, the molecular dipole moments extracted from A_J assuming the elementary Hönl-London factors are compatible among each other within experimental uncertainties. The weighted average of $\mu_0 = 0.982(15)$ D can be compared to calculations of the OH^- dipole moment. Values at the equilibrium internuclear distance are 1.050 to 1.072 D in earlier [25] and 1.10 D in recent work [29]. Taking the dipole moment function of Ref. [25], vibrational averaging reduces μ_0 by at most 0.04 D ($\mu_0 = 1.037$ D [18]). Hence, we find that current theory overestimates the OH^- dipole moment by $(5.3 \pm 1.5)\%$ and underestimates the OH^- rotational lifetimes by about $(10 \pm 3)\%$.

In the described time-dependent near-threshold photodetachment spectroscopy using a cryogenic storage ring,

TABLE I. Einstein coefficients, natural lifetimes τ_J, and the corresponding transition dipole moments measured for OH^- rotational states with the combined statistical and systematic uncertainty (1σ confidence level).

	$J = 1$	$J = 2$	$J = 3$	Unit
A_J	0.005 17(18)	0.0478(48)	0.189(13)	s^{-1}
$\tau_J = A_J^{-1}$	193(7)	20.9(2.1)	5.30(37)	s
μ_0	0.970(17)	0.952(48)	0.997(35)[a]	D

[a]Value used for $\mu_{0,J\geq 3}$.

the well-understood dynamics of *in vacuo* radiative relaxation allowed us to clearly identify the contributions of single rotational levels. This single-level sensitivity will be useful in the future to probe rotational population changes by in-ring molecular collisions. Moreover, a method was demonstrated to perform precise laboratory measurements of natural lifetimes and line intensities for extremely slow, purely rotational transitions in molecular ions. Rotational lifetimes from such measurements add a further, as-yet unavailable, experimental benchmark for quantum chemical calculations. Further improvements of the accuracy and applications to anionic molecules with more complicated rotational level structures can be envisaged.

Support by the Max Planck Förderstiftung is gratefully acknowledged. F. G., E. A. G., A. P. O., and H. K. were supported by the European Research Council under Grant No. StG 307163.

*Deceased.
†cmeyer@mpi-hd.mpg.de

[1] E. Herbst, Nature (London) **289**, 656 (1981).
[2] S. Petrie and E. Herbst, Astrophys. J. **491**, 210 (1997).
[3] M. C. McCarthy, C. A. Gottlieb, H. Gupta, and P. Thaddeus, Astrophys. J. **652**, L141 (2006).
[4] E. Bäckström, D. Hanstorp, O. M. Hole, M. Kaminska, R. F. Nascimento, M. Blom, M. Björkhage, A. Källberg, P. Löfgren, P. Reinhed, S. Rosén, A. Simonsson, R. D. Thomas, S. Mannervik, H. T. Schmidt, and H. Cederquist, Phys. Rev. Lett. **114**, 143003 (2015).
[5] R. von Hahn *et al.*, Rev. Sci. Instrum. **87**, 063115 (2016).
[6] A. P. O'Connor *et al.*, Phys. Rev. Lett. **116**, 113002 (2016).
[7] P. C. Engelking and D. R. Herrick, Phys. Rev. A **29**, 2425 (1984).
[8] J. R. Smith, J. B. Kim, and W. C. Lineberger, Phys. Rev. A **55**, 2036 (1997).
[9] P. A. Schulz, R. D. Mead, P. L. Jones, and W. C. Lineberger, J. Chem. Phys. **77**, 1153 (1982).
[10] F. Goldfarb, C. Drag, W. Chaibi, S. Kröger, C. Blondel, and C. Delsart, J. Chem. Phys. **122**, 014308 (2005).
[11] R. Otto, A. von Zastrow, T. Best, and R. Wester, Phys. Chem. Chem. Phys. **15**, 612 (2013).
[12] D. Hauser, S. Lee, F. Carelli, S. Spieler, O. Lakhmanskaya, E. S. Endres, S. S. Kumar, F. Gianturco, and R. Wester, Nat. Phys. **11**, 467 (2015).
[13] S. Menk, S. Das, K. Blaum, M. W. Froese, M. Lange, M. Mukherjee, R. Repnow, D. Schwalm, R. von Hahn, and A. Wolf, Phys. Rev. A **89**, 022502 (2014).
[14] Z. Amitay, D. Zajfman, and P. Forck, Phys. Rev. A **50**, 2304 (1994).
[15] P. Hlavenka, R. Otto, S. Trippel, J. Mikosch, M. Weidemüller, and R. Wester, J. Chem. Phys. **130**, 061105 (2009).
[16] H. Hotop, T. A. Patterson, and W. C. Lineberger, J. Chem. Phys. **60**, 1806 (1974).
[17] P. A. Schulz, R. D. Mead, and W. C. Lineberger, Phys. Rev. A **27**, 2229 (1983).
[18] See Supplemental Material at http://link.aps.org/supplemental/10.1103/PhysRevLett.119.023202 for methods, data analysis details, and numerical results, which includes Refs. [19–26].
[19] J. D. Rudmin, L. P. Ratliff, J. N. Yukich, and D. J. Larson, J. Phys. B **29**, L881 (1996).
[20] J. P. Maillard, J. Chauville, and A. W. Mantz, J. Mol. Spectrosc. **63**, 120 (1976).
[21] S. Gewurtz, H. Lew, and P. Flainek, Can. J. Phys. **53**, 1097 (1975).
[22] F. Breyer, P. Frey, and H. Hotop, Z. Phys. A **300**, 7 (1981).
[23] P. F. Bernath, *Spectra of Atoms and Molecules*, 2nd ed. (Oxford University Press, New York, 2005).
[24] Y.-P. Chang, F. Filsinger, B. G. Sartakov, and J. Küpper, Comput. Phys. Commun. **185**, 339 (2014).
[25] H. Werner, P. Rosmus, and E. Reinsch, J. Chem. Phys. **79**, 905 (1983).
[26] G. L. Molnár and R. B. Firestone, in *Handbook of Nuclear Chemistry*, edited by A. Vértes, S. Nagy, Z. Klencsár, R. G. Lovas, and F. Rösch (Springer, New York, 2011), pp. 475–610.
[27] L. M. Branscomb, Phys. Rev. **148**, 11 (1966).
[28] C. Blondel, W. Chaibi, C. Delsart, C. Drag, F. Goldfarb, and S. Kröger, Eur. Phys. J. D **33**, 335 (2005).
[29] B. S. D. R. Vamhindi and M. Nsangou, Mol. Phys. **114**, 2204 (2016).